PHILOSOPHICAL TRANSACTIONS OF THE ROYAL SOCIETY A MATHEMATICAL, PHYSICAL & ENGINEERING SCIENCES

Structure and Metamorphism of a Tectonically Thickened Continental Crust: The Yalu Tsangpo Suture Zone (Tibet)

J.-P. Burg, A. Leyreloup, J. Girardeau and G.-M. Chen

Phil. Trans. R. Soc. Lond. A 1987 **321**, 67-86
doi: 10.1098/rsta.1987.0005

Phil. Trans. R. Soc. Lond. A **321**, 67–86 (1987)

Printed in Great Britain

Structure and metamorphism of a tectonically thickened continental crust: the Yalu Tsangpo suture zone (Tibet)

By J.-P. Burg[1]†, A. Leyreloup[2], J. Girardeau[3] and Chen G.-M.[4]

[1] *Department of Geology, University of Melbourne, Parkville, Victoria* 3052, *Australia*

[2] *Laboratoire Pétrologie, U.S.T.L., Place Bataillon*, 34060 *Montpellier Cedex, France*

[3] *Institut de Physique du Globe, Université Paris* VI, 4 *Place Jussieu*, 75252 *Paris Cedex* 05, *France*

[4] *Department of Education, Ministry of Geology and Mineral Resources, Xisi, Beijing, People's Republic of China*

Three tectonic units (the active palaeomargin, the palaeo-oceanic domain and the passive palaeomargin) are now juxtaposed and constitute the Yalu Tsangpo suture zone between India and Eurasia in southern Tibet. We examine the deformation, metamorphic and uplift histories of each of these units. Our observations are accounted for in terms of the processes whereby the crust was thickened to about 70 km. We finally discuss the implications for ancient continental collision orogens.

Abbreviations

The following abbreviations are used in the text and figures:

act, actinolite	*kf*, K feldspar
alm, almandine	*ky*, kyanite
and, andalusite	*mu*, muscovite
ant, anthophyllite	*opx*, orthopyroxene
ap, apatite	*ore*, opaque
bi, biotite	*pl*, plagioclase
ca, carbonates	*phl*, phlogopite
cd, cordierite	*pre*, prehnite
ch, chlorite	*pyr*, pyrope
cpx, clinopyroxene	*qz*, quartz
ctd, chloritoid	*ru*, rutile
czo, clinozoisite	*sca*, scapolite
di, diopside	*sill*, sillimanite
do, dolomite	*sp*, spinel
ep, epidote	*spe*, spessartine
gr, graphite	*sph*, sphene
gro, grossular	*st*, staurolite
gt, garnet	*to*, tourmaline
hb, hornblende	*zo*, zoisite
ilm, ilmenite	*zr*, zircon.

† Present address: Centre Géologie et Géophysique, U.S.T.L., Place Bataillon, 34060 Montpellier Cedex, France.

Introduction

Tectonic processes involved in mountain building are controlled by the rheological behaviour of crustal materials, in particular ductile versus brittle deformation, which in turn is controlled largely by temperature and strain rate (Schmid 1982). Pressure–temperature–time (P–T–t) paths of rocks (England & Richardson 1977; England & Thompson 1984) are therefore fundamentally dependent on tectonic processes. However, the interaction between deformation and metamorphism is, at present, poorly understood, partly because there are relatively few constraints from field observations and/or regional geological syntheses to test and improve theoretical models. The aim of this paper is to consider the relation between patterns of regional metamorphism, deformation and the tectonic evolution of a modern collision zone. The example chosen is the Yalu Tsangpo suture zone, which is a segment of the type continent–continent collision orogen between India and Eurasia, figure 1. The structures (deformation) and metamorphism (thermal events) involved in collision and generation of an overthick continental crust will be described. These observations will be accounted for in terms of the geometry of the crustal thickening which metamorphic geologists deduce from P–T conditions and trajectories.

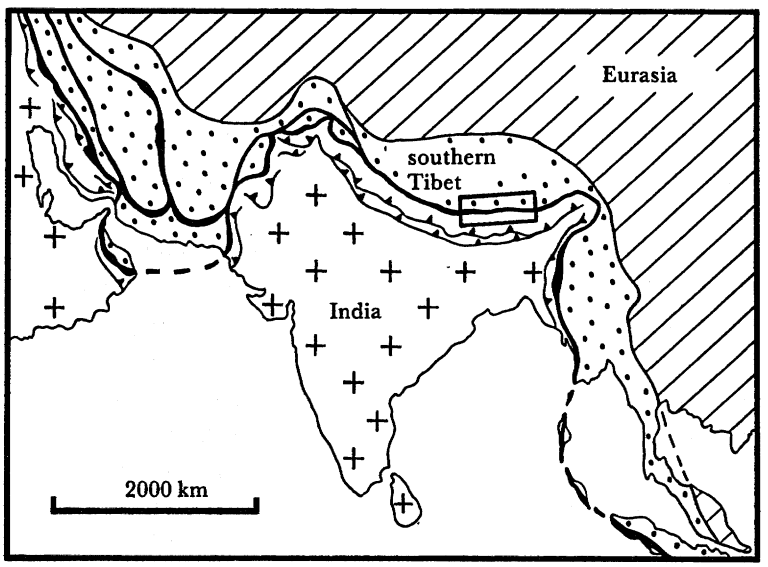

Figure 1. Location of the area studied. Ophiolite belts are shown in black. The southern Tibet and equivalent intermediate blocks are stippled.

Yalu Tsangpo suture zone: a collision history

The Yalu Tsangpo suture zone (figure 2) in southern Tibet (China) displays evidence of the complete plate tectonic cycle. An abbreviated geological history of the area, used as a background for this paper, is as follows.

1. Early stages of rifting and opening of the Neo-Tethys ocean between India and Tibet are recorded in Upper Permian and Lower Triassic exotic blocks contained in the olistostromic flysch (unit 6, figure 2; Burg *et al.* 1985).

2. Northward subduction of the Neo-Tethys oceanic lithosphere beneath southern Tibet promoted the production of a vast volume of magma. Dominantly I-type granitoids constitute

PHILOSOPHICAL TRANSACTIONS OF THE ROYAL SOCIETY A MATHEMATICAL, PHYSICAL & ENGINEERING SCIENCES

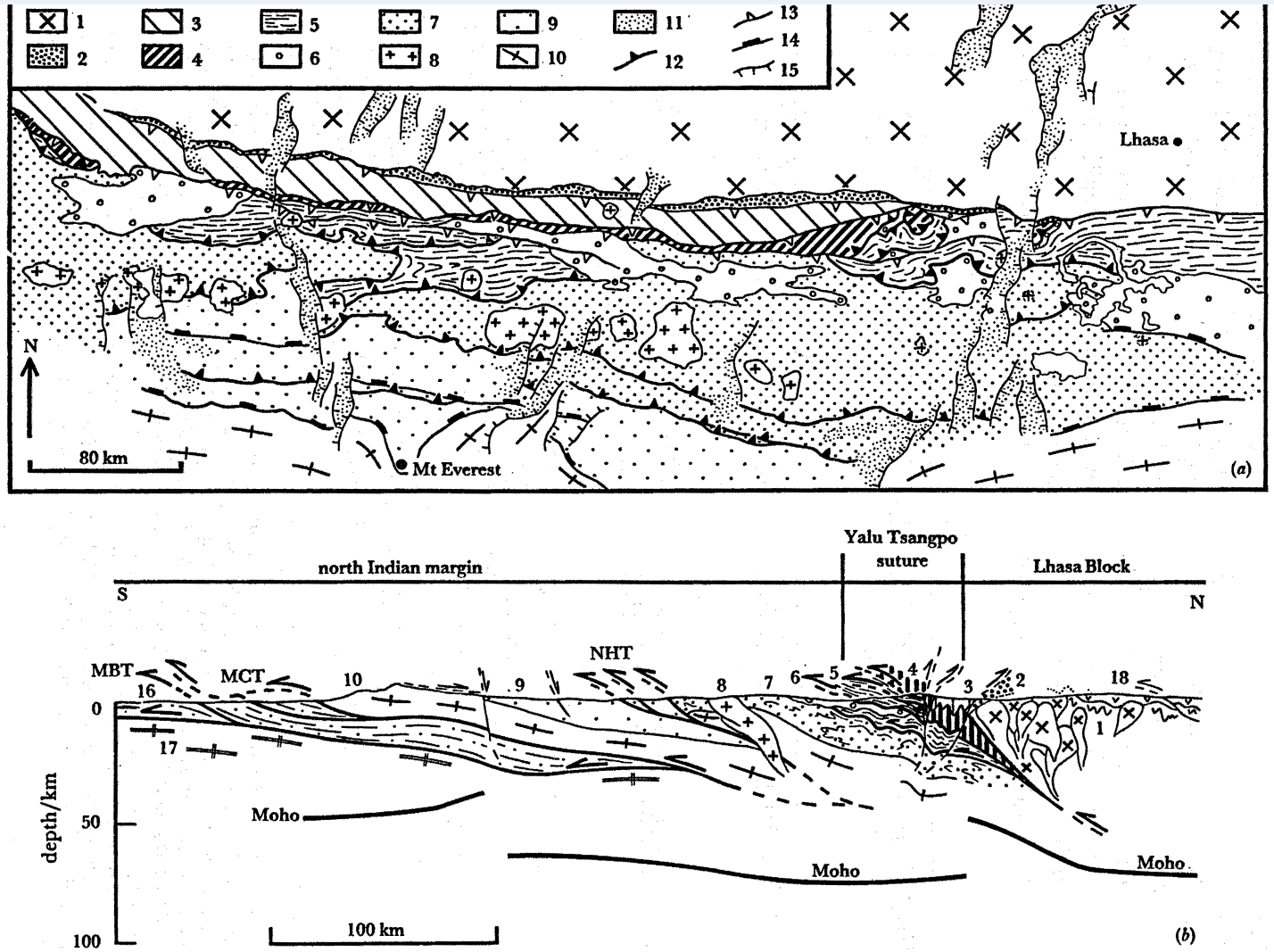

FIGURE 2. (*a*) Simplified geological map and (*b*) synthetic and interpretative cross section of the Yalu Tsangpo suture zone in southern Tibet, after Burg & Chen (1984), modified. Symbols: 1, Lhasa Block including the Plutonic Complex; 2, Eocene conglomerates; 3, Cretaceous to Palaeocene turbidites of the fore-arc basin; 4, Ophiolites; 5, Radiolarites and very low grade continental margin apron (turbidites); 6, unconformable flysch with exotic blocks; 7, north-Tethyan sediments; 8, north Himalayan two-mica granites and medium-grade crystalline rocks; 9, unmetamorphosed south-Tethyan sediments; 10, medium-grade to high-grade crystalline main central sheet, 11, Quaternary; 12, southward thrust; 13, post Oligo-miocene backthrust; 14, northward normal fault; 15, Quaternary normal faults; 16, gneiss and schists of the 'lesser Himalayas'; 17, Indian basement; 18, calc-alkaline unconformable lavas of the Lhasa Block. Abbreviations: NHT, north Himalayan thrust; MCT, main central thrust; MBT, main boundary thrust. Moho after Hirn *et al.* (1984*a*, *b*).

a long linear, multiple batholith spanning 120–40 Ma in age (Zhang, Y.-Q. *et al.* 1981; Maluski *et al.* 1982; Shärer *et al.* 1984). There is a close temporal and spatial relation with marginal continental-arc type volcanism (Coulon & Wang 1984).

3. Collision commenced in the lowermost Palaeocene with the arrival in the subduction zone of a strip of seamounts, pelagic horsts and the distal parts of the Indian continental margin now preserved as the exotic blocks. This event of *ca.* 60 Ma is accompanied by shear deformation of the northern Indian margin (Burg *et al.* 1985).

4. Continuing collision since the Eocene involved the development of imbricate thrust zones associated with intermediate-pressure metamorphism. The model (figure 3) implies thickening of the crust and the subsequent production of S-type granites (leucogranites) (Le Fort 1981; Dietrich & Gansser 1981). Later events include rejuvenation of the suture with post-Miocene backthrusting.

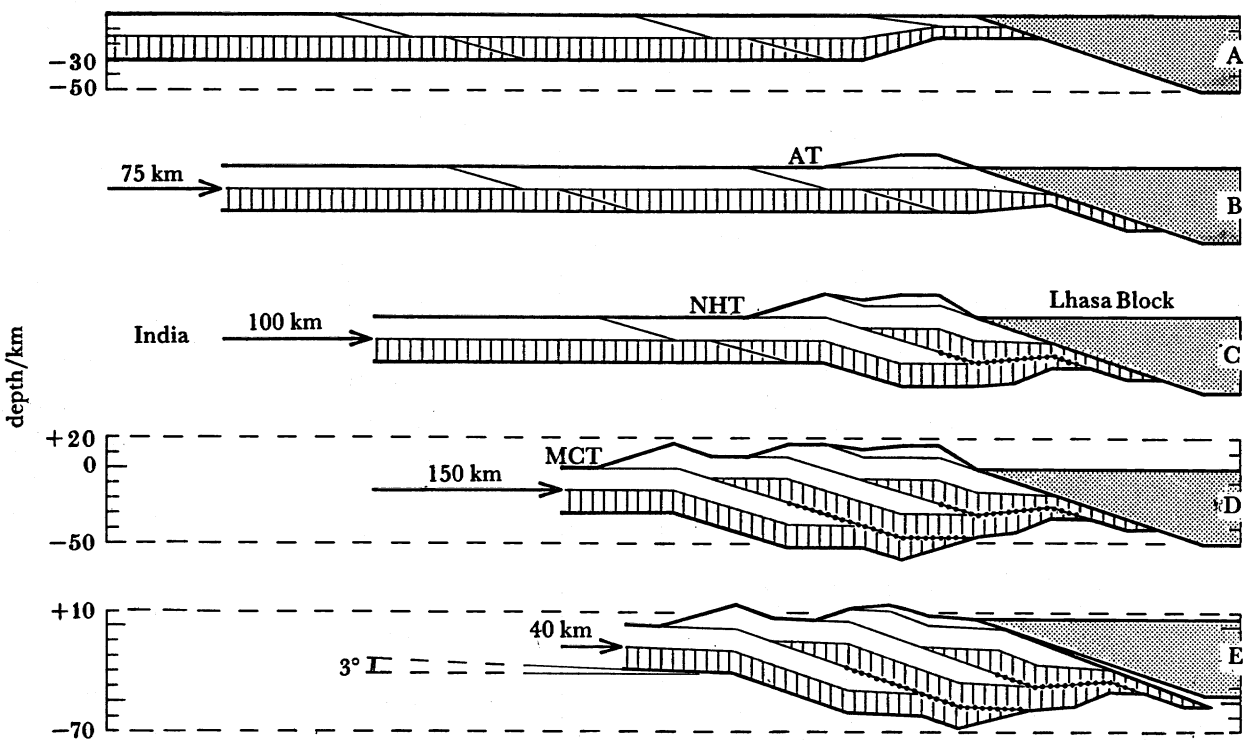

FIGURE 3. Equal area cross sections illustrating the structural model of the Yalu Tsangpo suture zone as commonly accepted in the literature (Shackleton 1981; Molnar 1984; Allègre *et al.* 1984). Stage A, 30 km thick Indian continental crust consists of a basement (hatched) and an upper sedimentary cover, both 15 km in thickness. The thinner continental margin is colliding (*ca.* 60 Ma) with a Lhasa Block already 50 km thick. Stages B, C, and D, (60–20 Ma) imbricate north-dipping thrust zones in the Indian continent climb from the Moho and decrease in age southward (AT, NHT, and MCT as in the text). Stage E is stage D with the Indian Moho at −70 km and the Lhasa Block height at +5 km (present day situation). A best fit is obtained after reactivation of the AT. The 3° tilt (bending of the lithosphere?, Karner & Watts 1983) is an unconstrained angle necessary to maintain the non-represented part of India at sea level. Ornamentation on thrusts indicates palaeo-Moho surfaces.

Both geological and palaeomagnetic data show that the southern edge of southern Tibet (Lhasa Block) had separated from Gondwana by the early Permian (Allègre *et al.* 1984). The Lhasa Block and a fore-arc basin formed the southern margin of continental Eurasia by the middle Cretaceous (*ca.* 110 Ma) (Pozzi *et al.* 1984) at a 10–20 °N palaeolatitude, while India

was still at 20–30 °S (Achache *et al.* 1984). India started to drift northward with respect to Eurasia at this time (Patriat *et al.* 1982).

Palaeomagnetism and detailed analysis of the magnetic anomalies in the Indian Ocean indicate that between 70 and 52 Ma (Upper Cretaceous to mid-Eocene) India drifted northward at a mean velocity of greater than 15 cm a^{-1}. At 52 Ma, relative and absolute motions began to exhibit several changes in direction. India rotated counter clockwise (*ca.* 35° and *ca.* 16° with respect to Eurasia and the Lhasa Block respectively), and a continuous decrease in the northward velocity is observed until 36 Ma (late Eocene). Since then India has resumed a stable northward motion with respect to Eurasia at a slower rate of *ca.* 5 cm a^{-1} (Patriat & Achache 1984). The erratic behaviour of India at 52 Ma is attributed to the onset of continental collision (Patriat & Achache 1984; Achache *et al.* 1984; Besse *et al.* 1984). After 52 Ma continuing collision involved some 1900 ± 850 km shortening north of the Lhasa Block, and 1400 ± 1200 km south of it (Achache *et al.* 1984) with less than 500 km of continental crust being subducted before the structure became inactive (Besse *et al.* 1984).

It can be seen therefore that metamorphism and deformation in the Yalu Tsangpo suture zone took place within a well-documented tectonic setting.

Structure and metamorphism of an overthick continental crust

In the Yalu Tsangpo suture zone, major crustal discontinuities (thrust faults) separate three tectonic units that have undergone different geological, deformation and metamorphic evolution (Burg & Chen 1984). They are, from north to south (figure 2):

(*a*) The active palaeomargin (Lhasa Block);

(*b*) The oceanic domain (Yalu Tsangpo suture);

(*c*) The passive palaeomargin (north Indian margin).

(*a*) *Active palaeomargin*

The active palaeomargin provides an example of plutonic magmatism (gabbros, two-pyroxene norites, diorites, granodiorites and granites) straddling a continental and oceanic plate boundary (Burg *et al.* 1983), with the plutonic locus remaining fixed from Upper Cretaceous until Eocene (120–40 Ma). Only in the mid-Eocene did magmatism spread northward to produce granites that intrude a pre-Himalayan crystalline crust (*mu*, *bi*, *st*, *gt* gneisses) and its sedimentary and volcanic cover, while I-type associations were produced within the main plutonic axis (Allègre *et al.* 1984). Large xenoliths of flaser gabbros, prasinites (amphibolites, deformed metadiorites and granodiorites), meta-volcanics, meta-cherts, metapelites, marbles and calc-silicate gneisses within the plutonic complex reflect the composition of the intruded crust. Xenoliths of ultramafics, mafic volcanics, cherts and carbonates have been interpreted as being derived from a metaophiolitic sequence of unknown age (Burg *et al.* 1983). South of the plutonic belt, the oceanic crust of the fore-arc basin (unit 3, figure 2) formed in the Upper Cretaceous, *ca.* 110 Ma (Marcoux *et al.* 1982; Göpel *et al.* 1984) and may be locally overlain by calc-alkaline lavas (Burg & Chen 1984).

Deformation history

A major backthrust now separates the Lhasa Block, the active palaeomargin to the north (figure 2), from the fore-arc basin of the oceanic domain to the south (unit 3, figure 2). In the Lhasa Block, deformation is characterized by a major regional upright folding event; in the southernmost regions this is superimposed onto earlier fabrics compatible with southward

thrusting (Burg *et al.* 1983). The upright folding implies 30 and 50% transverse shortening in the northern and southern regions respectively. This shortening took place between 80 and 60 Ma and is constrained by the age of folded and unconformable sequences (Burg *et al.* 1983; Achache *et al.* 1984). This is also the age of the arrival of seamounts and/or oceanic plateaus in the subduction zone (see above) that could be the driving mechanism (Nur & Ben-Avraham 1982) for the 'Andean'-type folding of the Lhasa Block. The unconformable series (unit 18, figure 2) comprising lavas 10 Ma old (H. Maluski & C. Coulon, personal communication) have undergone minor shortening (*ca.* 10%) and suggests recent shortening in Tibet, possibly of the same age as post-Oligomiocene backthrusting and associated folding of the Eocene conglomerates, which onlap the southern margin of the plutonic complex (unit 2, figure 2).

The fore-arc basin has been shortened 40–50% during one deformation phase, which post-dates the Lower Palaeocene *ca.* 60 Ma (Qian *et al.* 1982). The fore-arc sequence now occupies a synclinorium that is up to 50 km wide, thus indicating a minimum pre-deformational width of 80–100 km, which is similar in width to a young modern day fore-arc basin (Dickinson 1973). Localized deformations are associated with backthrusting on both sides of the synclinorium.

Metamorphic history

In the fore-arc sequences there is virtually no metamorphism.

Metamorphic assemblages we have recognized in the Lhasa Block are given in table 1. The metamorphism is of low-pressure type, spatially related to the proximity of the plutonic rocks. The steep metamorphic geotherm recorded by the metamorphic terrains may reflect successive accretion of mantle magmas (Wells 1980) during extension and/or strike-slip movements that are common in active continental margins (Tamaki 1985). Late fractures are infilled by *ca*, *pre*, *ch*, *bi*, *czo*, *ep* and rarely *act* in metatuffs and by *bi* and *hb* in amphibolites.

Uplift history

The uplift history coeval with and outlasting the construction of the active palaeomargin is constrained by several features.

(i) Upper Cretaceous (90–80 Ma) conglomerates in the fore-arc basin contain volcanic, plutonic and metamorphic rocks derived from the north (Shackleton 1981; Burg & Chen 1984). The magmatic belt was therefore being eroded at that time. Tectonic shortening being then at a minimum, this suggests that magmatic accretion was significantly rapid to generate overthickened crust in an Andean-style margin.

(ii) The upright folding event, between 80 and 60 Ma, could correspond to a rather homogeneous crustal shortening of a region that was characterized by a high thermal gradient. This folding was followed by erosion of a few kilometres (indicated by the deposition of subaerial ignimbrites on very low grade rocks; see, for example, Zhang, Q. *et al.* 1981; Burg *et al.* 1983).

(iii) Erosion of the magmatic belt, down to the currently exposed level, occurred in the Eocene (50–40 Ma) producing the voluminous molasse type conglomerates south of the Lhasa Block.

(iv) The exposure of low grade rocks on a regional scale, that constitute the Lhasa Block, imply very shallow erosion since the Eocene (less than 5 km correspond to less than *ca.* 10^{-1} mm a^{-1}).

There is no constraint on the uplift history of the fore-arc basin.

PHILOSOPHICAL TRANSACTIONS OF THE ROYAL SOCIETY A MATHEMATICAL, PHYSICAL & ENGINEERING SCIENCES

Table 1. Parageneses recognized in the Lhasa block

1, sedimentary cover pelites
† *qz*, *pl* (An_{0-30}), *kf* (Or_{85}) *mu*, *bi*, *cd*, *ilm*

2, large xenoliths pelites
† *qz*, *pl* (An_{43}), *kf* (Or_{90}), *mu*, (Ti)*bi*, *gt* (*alm*), *cd* (M/FM = 0.3), *and*, *sill* (fibrolite) Zn–*sp*, *ap*, *gr*, *to*, *ore*
† *qz*, *pl* (An_{40}), *kf* (Or_{90}), *mu*, (Ti)*bi*±*ch*, *and*, *cd*, *ap*, *gr*, *to*, *ore*
† ±*qz*±*pl* (An_{30-40}), (Ti)*bi*, *and*, *cd*, *sill* (fibrolite), Zn–*sp*, *gr*, *ore*

3, calc–silicate gneisses
† *qz*, *pl* (An_{70-80}), Ca-amphibole, *gt* (*gro*), *ep*, *sph*, *ore*
† *qz*, *pl* (An_{80}), *di*, Ca-amphibole, *zo*, *sph*, *ore*

4, marbles
† *qz*, *ca*, *di*, Ca-amphibole, *sca*, *ep*, *sph*, *ore*
† *qz*, *ca*, *ep*, *gt* (*gro*), idocrase, *sph*, *ore*
† *qz*, *ca*, *pl* (An_{70-80}), *ap*, *gt* (*gro*), *di*, Ca-amphibole, *sph*, *ore*
† *qz*, *ca*, *ep*, *di*, Ca-amphibole, *ch*, *sca*, *sph*, *ore*

5, cherts
qz, *ep*, amphibole (core = silicic-edenite to Mg-*hb*, rim = *act*-*hb* to *act*), *sph*, *ore*
qz, *czo*, *ep*

6, metabasalts or dolerites containing relictual augitic cpx, and brown hbl
qz, pl (An_{0-10}), amphibole (core = Mg-*hb*, rim = *act*) ±*bi*±*ch*, *ep*, *sph*, *ilm*, *ap*

7, metatuffs
qz, *pl* (An_{0-15}) ±*ch*±*mu*, *bi*, Mg-*hb*/*act*, *ep*/*czo*, *ilm*, *sph*, *ap*, pyrite
qz, *pl* (An_{0-15}), *bi*, *ep*, *sph*, *ilm*, *ap*±pyrite

8, prasinites and amphibolites (flaser gabbros, diorites and granodiorites)
pl (core = An_{50-55}, rim = An_{0-20}), Mg-*hb*/*act*, *ep*, *sph*, pumpellyite?, *ore*±*ap*
qz, *pl* (An_{0-15}), *ep*, Mg-*hb*/*act*±*bi*, *ilm*, *sph*, *ore*
qz, *pl* (An_{0-30}), Mg-*hb*, *bi*, *ch*, *ep*/*czo*, *sph*, *ilm*
† *qz*, *pl* (An_{30-35}), *hb*, *bi*, *ap*, *ore*
qz, *pl* (An_{10-20}), *kf*, Mg-*hb*/*act*, *bi*, *ore*, *zo*, allanite

	1		2		3			4			5		6	7				8		
	†	†	†	†	†	†	†	†	†	†									†	
qz	+	+	+	+/−	+	+	+	+	+	+	+	+	+		+		+	+	+	+
pl (An)	0–30	43	40	+/−30–40	70–80	80			70–80				0–10	0–15	0–15	0–15	0–15	0–30	30–35	10–20
kf (Or)	85	90	90																	+
ch			+/−	+/−						+			+/−					+		
mu	+	+	+																	
TiO2	< 1.6	2–4	2–4	< 1.6											+		+/−	+	+	+
bi													+/−							
M/FM	0.35	0.16–0.25	0.18–0.25	0.09																
gt		*alm*/*spe*			*gro*			*gro*	*gro*											
st (ZnO)																				
cd (M/FM)	0.48	0.3	0.3	0.1																
and		+	+	+																
ky																				
sill fibrolite		+		+																
sp (ZnO)		5–10		5–10																
di						+	+		+	+	Si–edenite									
amphiboles					Ca	Ca	Ca		Ca	Ca	Mg–*hb*/act		Mg–*hb*/*act*	Mg–*hb*/*act*		Mg–*hb*/*act*	Mg–*hb*/*act*	Mg–*hb*	Mg–*hb*	Mg–*hb*/*act*
ca							+	+	+	+										
epidote s.l.					*ep*	*zo*	*ep*	*ep*		*ep*	*ep*	*czo*/*ep*	*ep*	*czo*/*ep*	*ep*	*ep*	*czo*/*ep*			*zo*/allanite
ilm	+	+	+	+									+	+	+		+			
sph					+	+	+	+	+	+	+		+	+	+	+	+	+		
ap		+	+						+				+	+	+	+/−			+	
gr		+	+	+																
to		+																		
ores					+	+	+	+	+	+	martite			pyrite	+/−pyrite	+	+		+	+
Fe-sulphides				+																
others							*sca*	idocrase		*sca*						pumpellyite				

†, Low-pressure, medium- to high-temperature parageneses; low-pressure, low-temperature otherwise.

(*b*) *Oceanic domain*

Ophiolites and associated rocks

Ophiolites and radiolarites (units 4 and 5, figure 2) occur discontinuously along the Yalu Tsangpo suture zone: where they are absent, only backthrusts are found. The ophiolites have almost no cumulate gabbro and have a sill complex, rather than dykes, intruding serpentinized peridotites (Nicolas *et al.* 1981; Girardeau *et al.* 1985*a*). Sills and dykes indicate a primarily N 110° direction of palaeospreading (Pozzi *et al.* 1984) at 20–50° to the high-temperature plastic flow textures of the peridotites (Girardeau *et al.* 1985*b*). The sequence, which has locally preserved a normal polarity, is now underlain and separated from the radiolarites by a tectonic breccia and/or a serpentinite sole with blocks of rodingitized gabbro and dolerites, ophicalcites, amphibolites, marbles and quartzites.

Deformation and metamorphic history of the ophiolites

Crustal thickening was initiated in the oceanic domain. The low temperature schistose serpentinite sole contains high-temperature metamorphic rocks and locally overlies mylonitic peridotites indicating a southward thrusting emplacement (Girardeau *et al.* 1985*b*). The metamorphic rocks form pods of various size, often preserving gabbroic to doleritic magmatic textures. They include the following.

Garnet pyroxenites: *cpx* (Ca-rich augite), *gt* (almandine-rich, containing inclusions of *zo* and *czo*) ferroanpargasite to ferroanpargasitic *hb* (Leake 1978), and *ilm* derived from *sph*.

Garnet amphibolites: type 1, ferroanpargasite, almandine and type 2, ferroanpargasitic *hb* (50% of the rock) *gt* (almandine Fe-richer than in type 1 amphibolites), *pl* (An_{27}), *qz* and *ilm*.

Equilibrium temperatures for the garnet–pyroxenites indicate 800 °C < T < 1250 °C (geothermometers of Ganguly 1979; Powell 1985). Such estimates constrain a pressure of 6–9 kbar† (univariant transformation *sph–ilm*, grid of Spear 1981).

Besides the rare and localized saussuritization of oligoclase the rocks are very fresh. This suggests that cooling (hence uplift) was fast (faster than phase transformation rate). This rapidity is taken as other evidence for intra-oceanic thrusting which may have occurred when subduction took place at about 100–110 Ma.

A late brittle deformation event with *pre* and *qz* crystallized within fractures (90 °C < T < 250 °C; see, for example, Boles & Coombs 1977) indicates shallow conditions. The age of this cataclastic deformation could be anything between Palaeocene and the present.

Deformation and metamorphic history of the radiolarites and tuffs

The infra-ophiolitic radiolarite thrust slices, with tuffs and basaltic flows, exhibit a stretching lineation as part of polyphase deformation, indicating a tectonic transport from north to south (Burg & Chen 1984). Local high shear strain, represented by mylonites, also records a southward transport. Deformation occurred under greenschist facies conditions with a typical association: *qz* ± *pl* (An < 15), *ch*, *mu* ± *ep*, indicating 230 °C < T < 400 °C (Winkler 1974).

Blueschists, which are usually confined to convergent lithospheric plate boundaries (Coleman 1972; Ernst 1973), are known both to the west (Virdi *et al.* 1977; Virdi 1981) and to the east (Ghose & Singh 1980) of the studied area. However, the amphibole analyses published by Xiao

† 1 bar = 10^5 Pa.

& Gao (1984) have been erroneously identified as glaucophane. Analysis 5 is not an amphibole (too rich in Si); analyses 2, 3 and 4 are calc–sodic amphiboles (winchite to ferro-winchite, figure 4). The analysis 1, (assuming $K_2O = 0.5$ and not 6.5, which is incompatible with amphiboles and with the sum of oxides given in this paper) is an arfvedsonite (figure 4). Furthermore, lawsonite is characterized by Si:Al $\approx$ 1 and Ca:Al $\approx$ 0.5 (Deer *et al.* 1966). The 'lawsonite' analysed by Xiao & Gao (1984) is inconsistently specified by Si:Al $\approx$ 1.5 and Ca:Al $\approx$ 0.8. Therefore the association glaucophane–lawsonite in southern Tibet is yet to be found.

Arfvedsonite occurs in alkaline to calc-alkaline intrusions emplaced along the suture both within and south of the ophiolites (Burg & Chen 1984; Girardeau *et al.* 1985*a*). They are

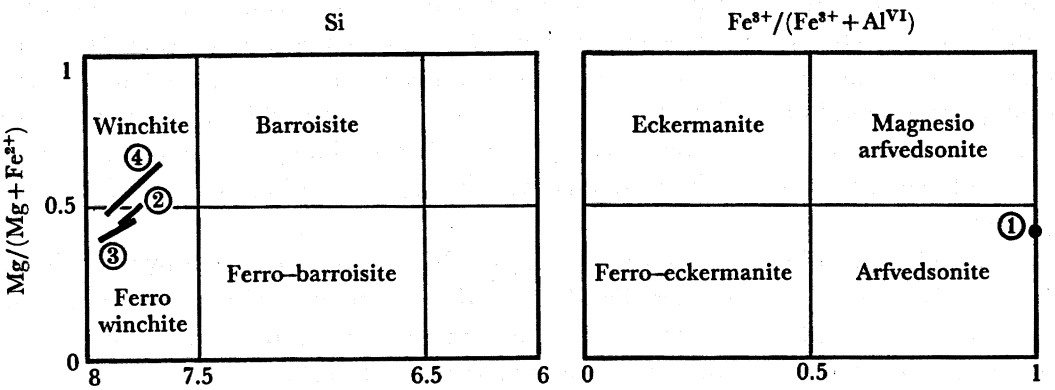

FIGURE 4. Plot of the 'glaucophane' analyses (circled numbers) published by Xiao & Gao (1984). Structural formulae calculated with 23 O; Fe^{3+} recalculated according to Papike *et al.* (1974). Analyses 2, 3 and 4 are characterized by $(Na+Ca)_B > 1.34$ with $1.34 > Na_B > 0.67$, $(Na+K)_A < 0.5$. Analysis 1 is characterized by $Na_B > 1.34$, $Na+K > 0.5$. Classification after Leake (1978).

gabbros, diorites, granodiorites and hypocrystalline granites that have developed contact aureoles in surrounding sedimentary rocks. Minerals associated with the contact metamorphism are *mu*, *ch*, *pre*, rarely pumpellyite, stilpnomelane and *gt*. They post-date any fabric of the rocks.

Uplift history

The uplift history of the suture rocks is difficult to ascertain. It probably involves a fast intraoceanic thrusting at *ca.* 110 Ma and an unknown (probably shallow) evolution until obduction when collision occurred at 60–50 Ma. Absence of blueschists supports the idea that crustal uplift in the central part of the suture is less important than at the extremities (Villotte *et al.* 1982). An unconformable polygenetic conglomerate lies on the suture rocks (Burg & Chen 1984) showing that by the Oligo-Miocene the suture rocks had been eroded to the present level.

(*c*) *Passive palaeomargin*

The lower-Palaeozoic to Cainozic continental shelf sediments of the Indian plate pass northward into deeper water facies with basic dykes and sills, presumably associated with continental rifting and the formation of a continental margin. The sediments now occur in three major and largely allochthonous tectonic entities, having been thrust southward towards the Indian foreland. From north to south, i.e. from top to bottom, the three imbricate units

are turbidites (continental margin apron), carbonaceous flysch (north-Tethyan sediments) and a platform sequence (south-Tethyan sediments) above the crystalline main central sheet (figures 2 and 3).

Deformation history

Large-scale recumbent folds, verging west to southwest, associated with a regional N–S to NE–SW stretching lineation developed in both the turbidite and carbonaceous flysch units (5 and 7 respectively, figure 2). The folds are responsible for inversion of the turbidite stratigraphy. The rocks contain a slaty cleavage formed in low-grade metamorphic conditions (typically involving *ch*, *mu*, *qz*, *pl* in pyrite-rich pelites). The intensity of the recumbent fabric decreases southward in the carbonaceous flysch. This tectono- metamorphic event is attributed to southward shearing and transport of lowermost Palaeocene age that folded limestones redeposited in the flysch with exotic blocks (6, figure 2); the flysch matrix is Lower Palaeocene in age (65–60 Ma) and unconformably lies on the recumbent fabric and related apron thrust (AT) contacts (figure 2; Burg *et al.* 1985). Both the recumbent fabric and the flysch with blocks are folded about E–W upright to south-facing tight folds containing a crenulation cleavage. The later folding event is locally contemporaneous with intrusion of north-Himalayan leucogranites.

In contrast to the turbidites and north-Tethyan sediments, the south-Tethyan sediments (unit 9, figure 2) are not metamorphosed and have suffered one main phase of E–W trending folds after the Eocene. Intensity of transverse shortening decreases southward and a faulted contact separates the sediments from the crystalline main central sheet.

Syntectonic metamorphic history

The north-Tethyan sediments show downward increasing metamorphism (table 2) from regional very low grade to localized medium-grade schists (Burg *et al.* 1984*b*). This is witnessed by the successive appearance in pelites of *mu*, *ctd*, *bi*, *gt*, *st*, *ky* and *sill* at the contact with the lowermost orthogneiss (Burg *et al.* 1984*b*). Deformed *ky* crystals are occasionally rimmed by euhedral *and*, suggesting rapid uplift followed intermediate high pressure type metamorphism related to crustal thickening along ductile thrust zones. The metamorphic rocks represent the more deeply eroded portions of an overthrust belt with a low dT/dP slope, intermediate-pressure type metamorphic zones (figure 5) spatially related to a ductile thrust zone. The deformation front of this southward thrust zone does not reach the upper part of the pile, but instead produces the north-Himalayan thrust (NHT) between the north- and south-Tethyan sediments. This is the consequence of the heterogeneity of the shear deformation during thrusting, which affects areas close to, and preserves the sequence away from, the thrust plane. In the deep-seated gneisses there was pre- to post-kinematic mineral growth with respect to the subhorizontal foliation and N–S lineation, in higher units syn- to post-kinematic growth. $^{40}Ar:^{39}Ar$ ages of micas are *ca.* 20 Ma (gneisses) and 13 Ma (schists) (H. Maluski, personal communication), that is, the same range as K:Ar conventional ages on *bi* (Debon *et al.* 1985).

The crystalline main central sheet (CMCT) is a metamorphic belt, 3.5–10 km thick, that is considered to represent Precambrian and Lower Palaeozoic rocks (Gansser 1964; Le Fort 1975), the age of which is thrown into dispute by *ky*-bearing gneisses in India in the CMCT that contain fossiliferous Jurassic rocks (Powell & Conaghan 1973). The CMCT has been extensively studied in Nepal and India where it has been thrust southward above the 'Lesser

PHILOSOPHICAL TRANSACTIONS OF THE ROYAL SOCIETY A MATHEMATICAL, PHYSICAL & ENGINEERING SCIENCES

Table 2. Parageneses recognized from top to bottom in the north Himalayan sediments

1, pelites

qz, *ch*, *pl* (?An_{10-30}), *mu*/phengite, *ilm*, *gr*, *ru* or anatase
qz, *ch*, *pl* (?An_{10-30}), *mu*/phengite, *ctd*, *ilm*, *gr*
qz, *ch*, *pl* (?An_{10-30}), *mu*/phengite, Fe–*bi*, *ilm*, *gr*
qz, *ch*, *pl* (?An_{10-30}), *mu*/phengite, *ctd*±*bi*, *ilm*, *gr*
qz, *ch*, *pl* (An_{25-30}), *mu*/phengite, *ctd*, *gt*, *st*, *ilm*, *gr*
qz, *pl* (An_{26-27}), *mu*, *bi*, *gt*±*zo*, *to*
qz, *pl* (An_{26-27}), *mu*, *bi*, *gt*, *st*, *to*, *ilm*
qz, *pl* (An_{24-25}), *mu*, *bi*, *gt*, *st*, *ky*, *ru*, *ilm*, *ap*, *to*±*zo*±*ca*
qz, *pl* (An_{29-32}), *mu*, *bi*, *gt*, *st*, *ky*, *sill*, *and*, *ilm*, *to*, *ap*±*zo*, Ti-magnetite

2, carbonaceous pelites

qz, *ch*, *mu*/phengite, *bi*, *ca*
qz, *ch*, *mu*/phengite, *pl* (An_{42-45}), *ca*, *ilm*, *gr*
qz, *ca*
qz, *pl* (An_{60-70}), *ca*, Mg–*hb*, *ilm*, *sph*
qz, *ca*, phlogopite, *mu*, *ru*±Ca–*pl*

3, basic rocks

qz, *pl* (An_{3-4}), *act* (core = Mg–*hb*), *ch*, *ep*, *ilm*, *sph*
ch, *act*, Mg–*hb*, *ant*, *czo*, *bi*, *mu*, *ilm*, *sph*
qz, *pl* (An_{84-88}), *kf*, Mg–*hb*, *gt*, *czo*, *ilm*, *sph*±*ch*
qz, *pl* (An_{85}), *kf*, Mg–*hb*, *ch*, *ilm*, *sph*
pl (An_{80-85}), Mg–*hb*, *bi*, *zo*, *sph*

4, orthogneiss

qz, *pl* (An_{20-25}), *kf* (Or_{87}), *mu*, *bi*, *zo*, *ilm*, *ru*, *ap*, *zr*

	1										2					3			4
qz	+	+	+	+	+	+	+	+	+	+	+	+	+	+		+	+		+
pl (An)	10–30	10–30	0–10			26–27	25–27	24–25	20–32		42–45		60–70	80	3–4		84–88	85	80–85	20–25
kf (Or)																	+	+		87
ch	+	+	+	+	+	+				+	+				+	+	+/−	+		
mu	+	+	+	+	+	+	+	+	+	+	+			+		+				+
TiO2					0.1	1.7		1.5	1.0	+										2.7–3.6
bi			Fe–	+/−	+/−		+									+			+	
M/FM					0.05	4.6		0.54	0.58											0.35
ctd		+		+	+															
gt					*alm*	*alm*	*alm*	*alm*	*alm*							*alm*				
st (ZnO)					1.4		+	<1	+											
cd (M/FM)																				
and									+											
ky								+	+											
sill fibrolite									+											
sp																				
di																				
amphiboles													Mg–*hb*		*act*/Mg–*hb*	*act*/Mg–*hb*/*ant*	Mg–*hb*	Mg–*hb*	Mg–*hb*	
ca								+/−		+	+	+	+	+						
epidote s.l.						+/−*zo*		+/−*zo*	+/−*zo*						*ep*	*czo*	*czo*		*zo*	*zo*
ilm	+	+	+	+	+		+	+	+		+		+		+	+	+	+		+
ores									magnetite											
Fe-sulphides											+/−	+/−	+/−	+/−						+
ap								+	+		+									
gr	+	+	+	+	+															
to						+	+	+	+											
sph													+		+	+	+	+	+	
others	*ru* anatase							*ru*						*ru* phlogopite						*ru* *zr*

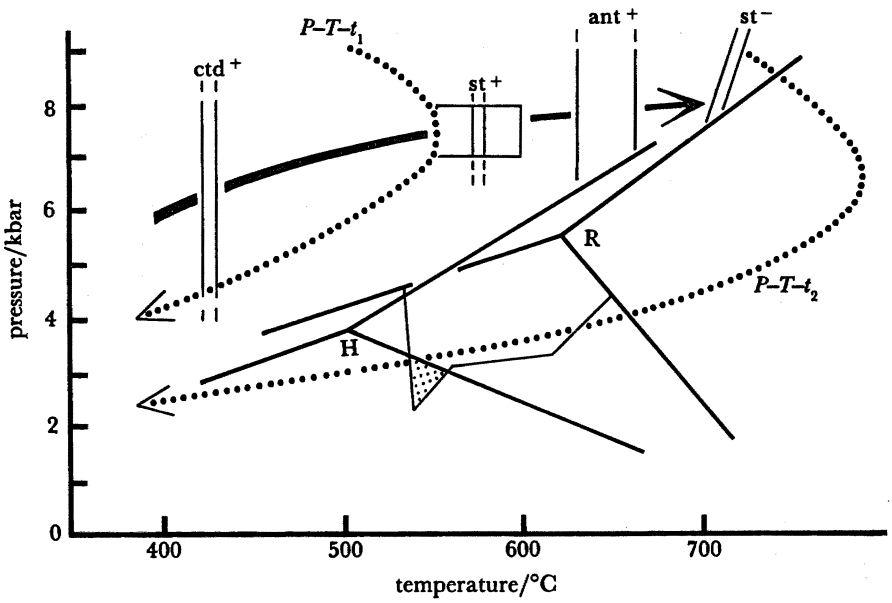

FIGURE 5. *P–T* array associated with the NHT: Al_2SiO_5 phase relations after H, Holdaway (1971) and R, Richardson *et al.* (1969) as modified by Powell (1978). *Ctd*$^+$, *st*$^+$ and *st*$^-$ after Hoschek (1969). Boxed areas are conditions determined by *bi–gt* geothermometer of Ferry & Spear (1978), *gt–pl* geobarometer of Ghent (1976), and *bi–mu–ch* geobarometer of Powell & Evans (1983). *Ant*$^+$ = *gt–hb* geothermometer of Graham & Powell (1984) containing *ant*$^+$ after Day & Halbach (1979). Stippled area is *gt–and–st* domain after Bickle & Archibald (1984). *P–T–t*$_1$ and *P–T–t*$_2$ are paths for a rock initially buried at 30 km with an average continental heat flux of 60 mW m^{-2} and 75 mW m^{-2} respectively. Thrust thickness = 20 km for *P–T–t*$_1$ (after figure 7*a* of England & Thompson 1984, uplift = 50 Ma, conductivity = 2.25 W m^{-1} k^{-1}) and = 35 km for *P–T–t*$_2$ (uplift = 100 Ma, conductivity = 1.5 W m^{-1} k^{-1} after figure 3*c*, same reference).

Himalaya', comprising Miocene rocks exposed in tectonic windows (Fuchs 1981). The position of the basal thrust (MCT) is disputed because in some places it is represented by a multiple thrust sequence (Sinha Roy 1982; Brunel 1983), and elsewhere by a wide shear zone (Bouchez & Pécher 1981). The assemblages found across the pile in Tibet are presented table 3.

The rocks bear evidence of multiple deformation and recrystallization events ascribed to Himalayan southward shearing, with the dominant fabric defined by the amphibolite facies assemblages (Pécher 1978; Thakur 1980; Brunel 1983). A medium-pressure type metamorphism (reverse close to and below the MCT; see, for example, Windley 1983; Arita 1983; Le Fort 1986) is synkinematic to the functioning of the MCT; it is a retrograde metamorphism superimposed on a previous 'Barrovian' or rather intermediate high-pressure type metamorphism: fibrolite postdating kyanite in *kf* (Or_{86}), *pl* (An_{30}), *gt*, *bi*, *ky* ± *sill* prismatic, *ru*, *gr* primary assemblages (see also Caby *et al.* 1983; Le Fort 1986), and retrogression of the *cpx–gt* basic granulites through the coronitic reaction $gt + qz + cpx \rightarrow opx + pl + hb \pm bi$. Late evolution towards higher temperature gradients is supported by voluminous anatexis in the middle of the pile. Pegmatite dykes, sometimes associated with the migmatites yet predating sillimanite crystallization, were emplaced after the development of tight folds. K:Ar absolute data on minerals and Rb:Sr on micas yield 30–12 Ma ages for the metamorphism (Krummenacher *et al.* 1978; Ferrara *et al.* 1983).

The fall in pressure may be attributed to (1) the rapid rate of uplift during thrusting and (2) to the tectonic denudation by gravity as discussed below.

PHILOSOPHICAL TRANSACTIONS OF THE ROYAL SOCIETY A MATHEMATICAL, PHYSICAL & ENGINEERING SCIENCES

TABLE 3. PARAGENESES RECOGNIZED FROM TOP TO BOTTOM ACROSS THE CMCT

1, pelites

† *qz*, *pl* (An_{10-12}), *mu*/phengite, *ch*, *gr*, *ap*, *to*, *zr*, *ores*
† *qz*, *pl* (An_{10-12}), *mu*/phengite, *bi*, *gr*, *ap*, *to*, *ores*
† *qz*, *pl* (An_{34-35}), *mu*, *bi*, *ctd*, *and*, *st*, *ap*, *zr*, *gr*, *to*, *ores*
† *qz*, *pl* (An_{26-30}), *mu*, *bi*, *st*, *ap*, *gr*, *to*, *ores*
† *qz*, *pl* (An_{22-33}), *mu*, *bi*, *gt*, *st*, *ap*, *gr*, *to*, *ores*
† *qz*, *pl* (An_{39-44}), *mu*, *bi*±*ch*, *gt*, *and*, *ap*, *gr*, *to*, *ores*
† *qz*, *pl* (An_{28-37}), *mu*, *bi*, *ch*, *gt*, *st*, *and*, *sill* (fibrolite), *ap*, *zr*, *gr*, *to*, *ores*
‡ *qz*, *pl* (An_{27-34}), *kf* (Or_{85-86}), *bi*, *gt*, *ky*, *sill* (prismatic), *ap*, *gr*, *zr*, *ores*
‡ *qz*, *bi*, *gt*, *sill* (prismatic and fibrolite), *ru*, *ap*, *zr*, *gr*, *ores*
qz, *pl* (An_{10-30}), *mu*, *bi*±*ch*, *sill* (fibrolite) ±*ru*±*gr*, *ap*, *zr*, *to*, *ores*
qz, *pl* (An_{21-26}), *mu*, *bi*, *gt*, *sill* (fibrolite), *ap*, *zr*, *to*, *ores*
qz, *pl* (An_{10-20}), *kf* (Or_{90}), *bi*±*ch*, *to*, *zr*, *ap*±*sph*, *ores*
qz, *pl* (An_{1-3}), *kf* (Or_{90-93}), *mu*, *bi*, *gt*, *sill* (fibrolite), *zr*, *ap*, *ores*
qz, *pl* (An_{1-9}), *kf* (Or_{93}), *mu*, *bi*±*ch*, *to*, *zr*, *ap*, *ores*
qz, *pl* (An_{7-8}), *kf* (Or_{90-95}), *mu*, *bi*±*ch*, *gt*, *ap*, *zr*, *to*, *ores*
qz, *pl* (An_{25-30}), *mu*, *bi*, *ilm*, Ti-magnetite, *ap*, *zr*, *to*

2, metacarbonates

† *qz*, *pl* (An_{30-40}), *ca*, *ep*, *sph*, *ores*
† *ca*, *do*, *qz*, *mu*
† *ca*, *qz*, *ch*, *gt*±*hb*±*bi*, *czo*, *pl* (An_{90})+*sca*
† *ca*, *qz*, *di*, *czo*
† *ca*, *qz*, *mu*±*hb*, *phl*, ep±di±*gt* (*gro*)
‡ *qz*, *pl* (An_{97}), *di*, *gt* (*gro*), *ep*, *sph*, *ore*
† *ca*, *qz*, *ch*, *pl* (An_{90}), *mu*, *ilm*, *gr*

3, metabasic rocks

‡ *hb*±*bi*, *pl* (An_{38})±*gt*±*qz*±*sp*±*zo*±*ch*, second generation *pl* (An_{53-57})
† *hb*, *cpx*±*opx*, *bi*±*gt*±*qz*, second generation *pl* (An_{83-96})
hb, *pl* (An_{50-60}) *sph*, *ap*, *ores*

	1																			2							3	
	†	†	†	†	†	†	†	‡	‡											†	†	†	†	†	‡	†	‡	
	+	+	+	+	+	+	+	+	+	+	+	+	+	+	+	+	+	+	+	+	+	+	+	+	+	+	‡ +	
)	10–12	10–12	34–35	28–30	22–33	39–44	28–37	27–34		10–30	21–26	10–20	0.8–6	1–9	7–8	11–15	100–26	40–30		90			97	90	38–57	83–96	50–60
)								85–86		85		90	89–94	93	90–95			97									
	+	+/−	+			+	+					+/−		+/−	+/−					+		+	+				
	+	+	+	+	+	+	+			+/−	/−	+	+	+	+	+	+		+			+		+			
02			0.6–2.0	1–1.4			1.5–2.7	3.9–5	3.8–5.7	3–3.4	0.1–3.4	1.5–3	0–3.8	2–2.6	2–2.7	1.5												
		+	+/−														+			+/−					+/−	+	
FM				0.34–0.42			0.36–0.41	0.52–0.56	0.46–0.60	0.45	0.27–0.37	0.28–0.33	0.25–0.31	0.2–0.39	0.19–0.22	0.52												
			+																									
				alm	*alm*		*alm*	*alm/pyr*	*alm/pyr*		*alm/pyr*		*alm/spe*		*alm/spe*		*alm/gro*			*alm/gro*			+/-*gro*	*gro*		*alm/ pyr/gro*	*alm/ pyr/gro*	
O)			0.8–1.0	< 0.6	< 0.20	0.6	< 0.5																					
/FM																												
			+			+	+																					
								+	fibr																			
							fibr	prism	prism	fibr	fibr		fibr															
																										+		
iboles																	hornblende			+/−*hb*			+/−	+		*hb*	*hb*	*hb*
																	+				+							
te s.l.								+	+	+						+	*zo*/allanite	*ep*		*czo*	*czo*	*ep*	*ep*			*zo*		
	+	+	+	+	+	+	+				+	+	+	+	+		+	+						+				+
lphides	+	+	+	+	+	+	+	+	+	+	+	+	+	+	+	+	+											+
	+	+	+	+	+	+	+	+	+	+	+	+		+	+	+												
	+		+					+	+	+	+	+	+	+		+	+			+/−*sca*		phlogopite	+/−*sca*			*opx/cpx*		
									ru	*ru*	+/−*ru*					Ti *magnet.*												

†, Low-pressure, high-temperature parageneses; ‡, high-pressure granulites; intermediate-pressure type metamorphism otherwise.

Magmatic history

Tourmaline and two mica-bearing leucogranites are prominent both across the NHT (north-Himalayan Belt; see, for example, Debon *et al.* 1983, Burg *et al.* 1984*b*) and within the upper part of the CMCT (Dietrich & Gansser 1981; Le Fort 1986). In the intrusions of the CMCT, Rb:Sr isotopes give mineral ages of 31–12 Ma and high initial $^{87}Sr:^{86}Sr$ ratios, implying anatectic melting of Palaeozoïc or older crustal rocks (Krummenacher 1971; Dietrich & Gansser 1981; Vidal *et al.* 1982; Ferrara *et al.* 1983). The contact aureoles in the country rocks involve crystallization of *mu*, *bi* or *ctd*, *gt* (with a progade temperature zoning), *st* and *and* in the pelites, and of *gt*, *di* and *sca* in carbonates. A *sill–cd* association has been reported by Brunel & Kienast (1986).

Leucogranites of the north-Himalayan belt have the same characteristics as those of the CMCT (Wang *et al.* 1981; Debon *et al.* 1983). K:Ar and Rb:Sr mineral ages yield 7–15 Ma (Zhang Y. Q. *et al.* 1981; Debon *et al.* 1983, 1985), also obtained by $^{40}Ar:^{39}Ar$ and by U:Pb on zircon (H. Maluski & U. Shärer, personal communication). The contact aureoles involve crystallization of *ch* and equant lath-shaped *ctd*; *cd* and exceptional occurrences of *and* (chiastolite) grown after *gt* and *st* are found. One of these plutons has intruded the fore-arc basin, suggesting that a continental crust underlies the sequence.

Uplift history

The deeper rocks found close to the NHT were metamorphosed in the range 600–700 °C, and 7–8.5 kbar (figure 5). These peak conditions are not attained in *P–T–t* paths computed for an average surface heat flow (England & Thompson 1984). Consequently they imply a rather high heat supply distribution, which would be consistent with *and* rimming *ky* along the uplift path (figure 5). Geothermobarometry applied to zoned garnets close to the MCT indicates equilibration *P–T* conditions of 640–850 °C, 6–7 kbar for the core, and 440–630 °C, 4–5 kbar for the rim (figure 6; see also Brunel & Kienast 1986). The NHT and the MCT have therefore undergone uplift of about 30 km in *ca.* 20 Ma. However, both regions may differ in their cooling history.

The NHT region has been thrust before emplacement of *ca.* 10 Ma cross-cutting leucogranites (8, figure 2). Intrusions were relatively shallow (3–4 kbar = *ca.* 10 km, contact *ch*, *ctd*, *gt* and *st* are common, *and–cd* exceptional), suggesting the region was uplifting and being eroded at the time of magmatic emplacement, essentially in response to crustal thickening. Rocks overlying the thrust plane cooled rapidly after the thrusting event (exhumation rate *ca.* 1.5 mm a^{-1}) and may not subsequently have attained temperatures higher than their initial ones as inferred on computed *P–T–t* paths (England & Thompson 1984).

Perfectly preserved 'Barrovian'-to-intermediate high-pressure metamorphic assemblages in the CMCT suggest that at least part of it was uplifted as a near rigid block. Penetrative deformation at *P–T* conditions along the uplift path would be expected to have catalysed retrograde greenschist reactions. The retrograde products are within 1 to 50 cm thick diaphthoritic (*mu*, *ch*, *pl* (An < 20), *qz* ± *ep*) phyllonite zones that parallel the regional foliation. These zones represent post-metamorphic southward reverse faults, which were active in the exhumation process.

Important normal faulting (greater than 7 km vertical downthrow of the south-Tethyan sediments), and therefore active denudation above the CMCT, is evidenced by shear-fabrics

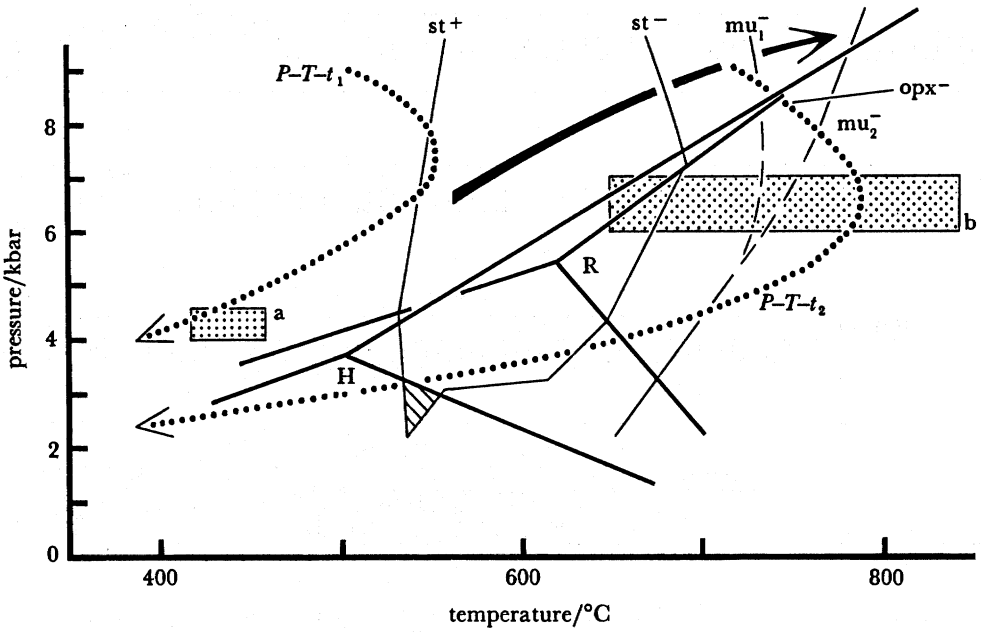

FIGURE 6. *P–T* array associated with the CMCT: H and R triple points, *gt–and–st* domain, P–T–t_1 and P–T–t_2 as in figure 5. St^+ and st^- after Bickle & Archibald (1984). Mu^- after Storre (1972), (1) = $P_{H_2O} < 2$ kbar and (2) = $P_{H_2O} = P_T$. $Opx^- = gt + qz \rightarrow opx + pl$. Stippled boxes respresent *gt–bi* geothermometer and *gt–pl* geobarometer as in figure 5 on *a*, core of zoned garnets and *b*, non-zoned garnets both close to the MCT. Hatched area is contact metamorphism of leucogranites in the upper part of the CMCT.

and crystallographic preferred orientations developed within the leucogranites, and is responsible for north-facing folds in the south-Tethyan sediments (Burg *et al.* 1984*a*). The normal faulting accounts for unmetamorphosed palaeozoic rocks lying on metamorphic rocks along the northern boundary of the CMCT, and is bracketed in age between the leucogranites emplacement (*ca.* 20 Ma) and the Pleistocene (*ca.* 5 Ma). Uplift of the CMCT is partitioned between a response to crustal thickening by erosion and a vertical displacement, due to both reverse faulting within the pile and tectonic denudation. The resulting fast cooling can be responsible for preserving the transitional S-shape of the isograds below the MCT (Le Fort 1975; Pécher 1978) possibly accentuated by later movements within the reverse phyllonitic zones.

Present-day situation

The major thrust sheets (MCT and NHT) correspond to the prism-shaped seismic structures reported by Hirn *et al.* (1984*a*, *b*), implying decoupled lower and upper crustal layers. The superposition of neighbouring segments in the lower crust occurs along imbricate thrusts involving upper-mantle rocks with polarity opposed to thrusts in the upper crust (figure 7). This paradox in geometry could explain marked steps in the Moho surface (figure 2*b*), although recent faulting might be the controlling factor (Hirn *et al.* 1984*b*; Burg & Chen 1984). In any case, both interpretations disagree with crustal thickening occurring through mere underplating of several hundred kilometres of continuous Indian crust beneath Tibet (Powell & Conaghan 1975). An effective test of the paradoxical model is to reconcile its erosional product with the eroded model of figure 2 (figure 8). Erosion in the classical model leads to

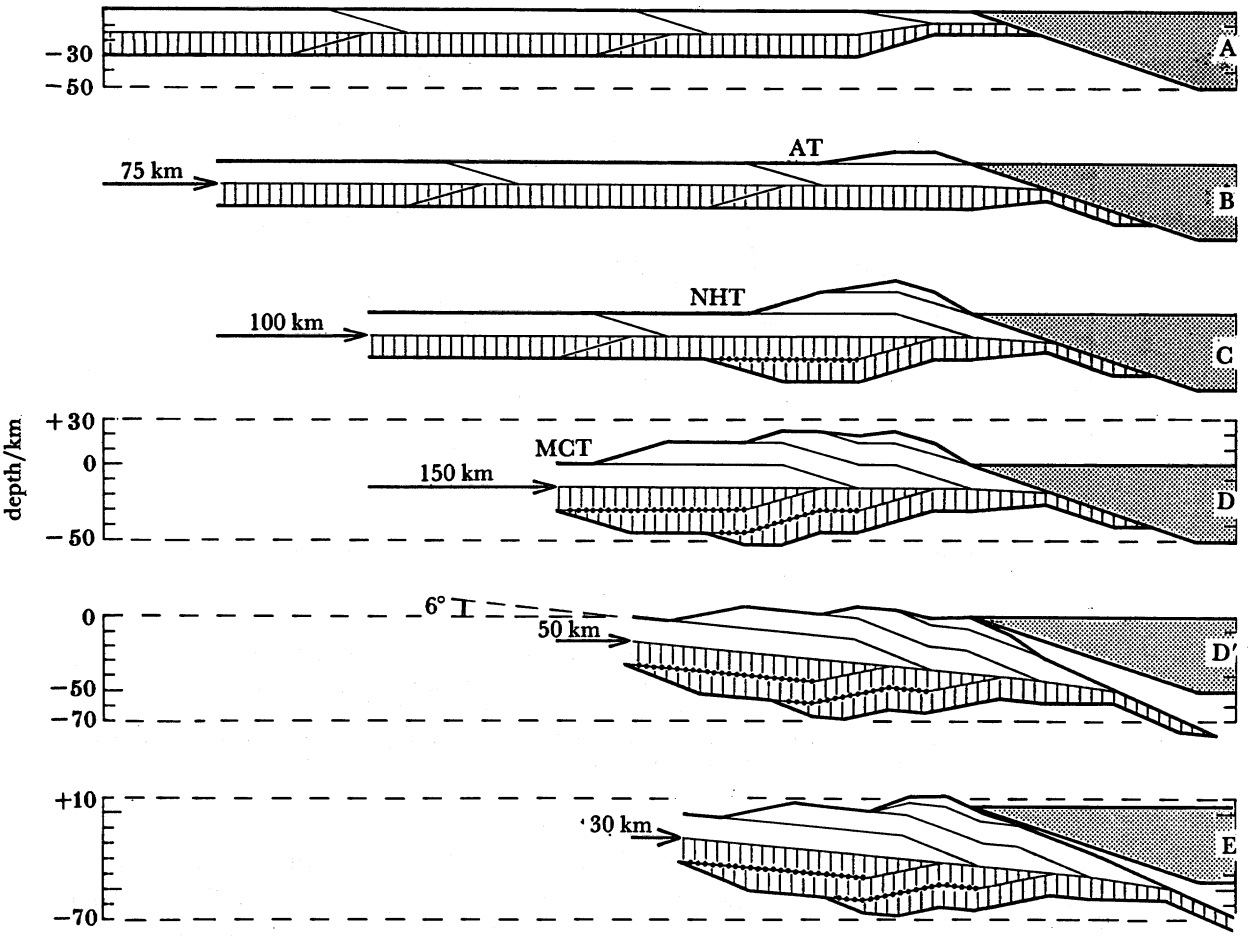

FIGURE 7. Paradoxical structural model based on seismic profiles (Hirn *et al.* 1984*a*, *b*). Legend as in figure 2. Note that the same succession of events allows more bending and consequently more shortening (stage D′) than in the model of figure 3.

exposure of palaeo-Moho and alternation of lower-crust and cover belts; the paradoxical model favours widespread outcrops of lower-crust (reworked ?) material and does not allow the continental Moho to be exposed. Conversely, cover rocks only would be exposed with erosion 5 km less than that involved in figure 8, a case that is strongly reminiscent of the Caledonian and Variscan belts in Europe. These are points which obviously may be of some consequence when studying an ancient and deeply eroded orogenic belt. Here two different types of orogenic belts are presented, which actually depend upon the rheological response of the lower (ductile) part of the crust. This aspect could be the major controlling factor in the final structure of any orogen.

Another point of interest is the present-day high heat flow ascribed to a shallow (less than 10 km) and recent source (Jaupart *et al.* 1985). The heat-flow data provide evidence that melting processes are widespread and still active in the Tibetan crust, 50 Ma after collision. This is obviously important for the late tectono-metamorphic evolution of a collision belt. It would suggest that terrains in which S-type plutonism is the most recent thermal and tectonic event may be associated with an intracontinental, post-collisional evolution.

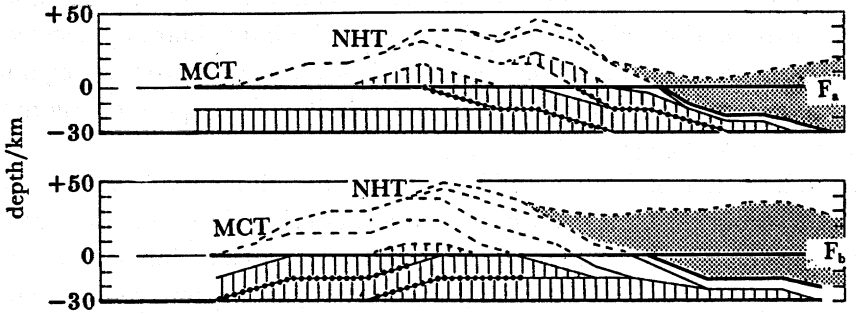

FIGURE 8. Erosional results (F for future) of the classical model F_a and the paradoxical model F_b. Same legend as figure 3.

Finally, crustal thickening does not now occur in southern Tibet. Extension tectonics are still very active producing N–S grabens (Tapponnier *et al.* 1981; figure 2*a*), the probable surface response to deep-level spreading due to gravitational body forces (England & McKenzie 1982, 1983). This thinning process may be of some consequence for the present uplift rate.

CONCLUSIONS

In the Yalu Tsangpo suture zone, *P–T–t* paths and deformation styles are associated with contrasting histories between different tectonic units.

In the active palaeomargin, calc-alkaline magmatism was accompanied by significant pre-collision thickening. As a consequence, thermal gradients were elevated above the steady-state geotherm favouring a relatively homogeneous shortening and associated thickening contemporaneous with collision with oceanic plateaus. Erosion took place shortly after this event enhanced by isostatic equilibration of the magmatically thickened crust. This is marked by the Palaeocene unconformity in the Lhasa region. The Lhasa Block and the fore-arc basin represent the overriding plate whose deformation is substantially less than that of the subducted plate at the time of collision.

In the passive palaeomargin, moderate-to-low geothermal gradients accompanied the crustal thickening episode (collision and obduction?). This may have increased the total radiogenic heat production in a given vertical column, thus, with heating, allowing anatexis and S-type granite generation. Continued collision developed heterogeneous shear strain with upward and downward decreasing deformation in the hanging and foot walls of the thrust zones. This is why a deformation pause may be represented by an unconformity (in Tibet the flysch with blocks), although it is not necessarily an orogenic pause as shearing may develop in the lower parts of the crust. Thrusting led to crustal stacking, which affected more and more external areas with a regional stretching lineation that coincides with the relative motions of the converging crustal segments. High-grade rocks have been brought to the surface along the major thrust zones; these dip in the same sense as the initial subduction in the upper part of the crust and form characteristic belts of metamorphic and deformational facies. Exposure of high-grade rocks is therefore caused as much by tilting of the crust as by uplift consequent upon the erosion induced by tectonic burial. There is no evidence that a phase of isobaric heating exists between the assembly of the orogen as a thrust system and the onset of erosion

PHILOSOPHICAL TRANSACTIONS OF THE ROYAL SOCIETY A MATHEMATICAL, PHYSICAL & ENGINEERING SCIENCES

of that pile. The rapidly thickened crust experiences 'collapse', which is additional to the erosion process for exhumation of deeper rocks. The uplift path follows a clockwise high geothermal gradient. Late and abundant leucogranites associated with a regional high-temperature metamorphic overprint appear to be a hallmark of post collisional crustal shortening (Dewey & Burke 1973).

With only a few kilometres of further uplift, the ophiolitic klippen will be eroded leaving little evidence in the orogenic belt of former oceanic material. Based on the premise that similarity is not coincidence, but is the result of a sequence of events inherent to any major continental collision, we believe that, in ancient orogenic belts, distinctions comparable to those described in this essay between different domains will help in interpreting some stages of paleo-continental collisions.

The field work was carried out within the Cooperative Research Project of the Chinese Ministry of Geology, Chinese Academy of Sciences, French Centre National de la Recherche Scientifique and Institut National d'Astronomie et de Géophysique. We thank F. Proust, R. Caby, M. Guiraud and F. Romney for helpful discussions. C. J. L. Wilson, R. Powell and M. Sandiford improved our manuscript.

References

Achache, J., Courtillot, V. & Zhou, Y.-X. 1984 *J. geophys. Res.* **89**, 10311–10339.

Allègre, C. J., Courtillot, V., Tapponnier, P., Hirn, A., Mattauer, M., Coulon, C., Jaeger, J.-J., Achache, J., Shärer, U., Marcoux, J., Burg, J.-P., Girardeau, J., Armijo, R., Gariepy, C., Göpel, C., Li, T. D., Xiao, X.-C., Chang, C.-F., Li, G., Lin, B., Teng, J., Wang, N., Chen, G., Han, T., Wang, X., Den, W., Sheng, H., Zao, Y., Zhou, J., Qui, H., Bao, P., Wang, S., Wang, B., Zhou, Y. & Xu, R. 1984 *Nature, Lond.* **307**, 17–22.

Arita, K. 1983 *Tectonophysics* **95**, 43–60.

Besse, J., Courtillot, V., Pozzi, J.-P., Westphal, M. & Zhou, Y.-X. 1984 *Nature, Lond.* **311**, 621–626.

Bickle, M. J. & Archibald, N. J. 1984 *J. metamorph. Geol.* **2**, 179–203.

Boles, J. R. & Coombs, D. S. 1977 *Am. J. Sci.* **277**, 982–1012.

Bouchez, J. L. & Pécher, A. 1981 *Tectonophysics* **78**, 23–50.

Brunel, M. 1983 Etude pétro-structurale des chevauchements ductiles en Himalaya (Népal oriental et Himalaya du Nord-Ouest). (395 pages.) Thèse d'État Paris VII.

Brunel, M. & Kienast, J.-R. 1986 *Can. J. Earth Sci.* (In the press.)

Burg, J.-P., Brunel, M., Gapais, D., Chen, G. M. & Liu, G. H. 1984*a* *J. struct. Geol.* **6**, 535–542.

Burg, J.-P. & Chen, G.-M. 1984 *Nature* **311**, 219–223.

Burg, J.-P., Guiraud, M., Chen, G. M. & Li, G. C. 1984*b* *Earth planet. Sci. Lett.* **69**, 391–400.

Burg, J.-P., Marcoux, J. & Cheng, G.-M. 1985 *Terra Cognita* **5**, 125.

Burg, J.-P., Proust, F., Tapponnier, P. & Chen, G. M. 1983 *Eclog. geol. helv.* **76**, 643–665.

Caby, R., Pécher, A. & Le Fort, P. 1983 *Revue Géogr. phys. Géol. dyn.* **24**, 89–100.

Coleman, R. G. 1972 Blueschist metamorphism and plate tectonics. *Rep.* 24th *Int. Geol. congr.*, sect. 2, pp. 19–26.

Coulon, C. & Wang, S. 1984 Caractèristiques du volcanisme du Tibet Central et méridional. Implications géodynamiques. *Himalayan Geology. Int. Symp.*, Abstracts. Chengdu, China.

Day, H. W. & Halbach, H. 1979 *Am. Miner.* **64**, 809–823.

Debon, F., Sonet, J., Liu, G. H., Jin, G. W. & Xu, R. H. 1983 *C. r. hebd. Séanc. Acad. Sci., Paris* (*II*) **295**, 213–218.

Debon, F., Zimmermann, J.-L., Liu, G.-H., Jin, C.-W. & Xu, R.-H. 1985 *Geol. Rdsch.* **74**, 229–236.

Deer, W. A., Howie, R. A. & Zussman, J. 1966 *An introduction to the rock-forming minerals.* (528 pages.) London: Longman Group Limited.

Dewey, J. F. & Burke, K. C. A. 1973 *J. Geol.* **81**, 683–692.

Dickinson, W. R. 1973 *J. geophys. Res.* **78**, 3376–3389.

Dietrich, V. & Gansser, A. 1981 *Schweiz. miner. petrogr. Mitt.* **61**, 177–202.

England, P. C. & McKenzie, D. 1982 *Geophys. Jl R. astr. Soc.* **70**, 295–321.

England, P. C. & McKenzie, D. 1983 *Geophys. Jl R. astr. Soc.* **73**, 523–532.

England, P. C. & Richardson, S. W. 1977 *J. geol. Soc. Lond.* **134**, 201–213.

England, P. C., Thompson, A. B. 1984 *J. Petr.* **25**, 894–928.

Ernst, W. G. 1973 *Tectonophysics* **26**, 229–246.

PHILOSOPHICAL TRANSACTIONS OF THE ROYAL SOCIETY A MATHEMATICAL, PHYSICAL & ENGINEERING SCIENCES

Ferrara, G., Lombardo, B. & Tonarini, S. 1983 *Geol. Rdsch.* **72**, 119–136.
Ferry, J. M. & Spear F. S. 1978 *Contr. Miner. Petr.* **66**, 113–117.
Fuchs, G. 1981 *Mitt. öst. geol. Ges.* **74/75**, 101–127.
Ganguly, J. 1979 *Geochim. cosmochim. Acta* **43**, 1021–1029.
Gansser, A. 1964 *Geology of the Himalayas.* (289 pages.) London: Wiley-Interscience.
Ghent, E. D. 1976 *Am. Miner.* **61**, 710–714.
Ghose, N. C. & Singh, R. N. 1980 *Geol. rdsch.* **69**, 41–48.
Girardeau, J., Mercier, J.-C. & Wang, X. 1985*a* *Contr. Miner. Petr.* **90**, 309–321.
Girardeau, J., Mercier, J.-C. C. & Yougong, Z. 1985*b* *Tectonophysics* **119**, 407–433.
Göpel, Ch., Allègre, C. J. & Xu, R.-H. 1984 *Earth planet. Sci. Lett.* **69**, 301–310.
Graham, C. M. & Powell, R. 1984 *J. metamorph. Geol.* **2**, 13–31.
Hirn, A., Lépine, J. C., Jobert, G., Sapin, M., Wittlinger, G., Xu, Z.-X., Gao, E.-Y., Wang, X.-J., Teng, J.-W., Xiong, S.-B., Pandey, M. R. & Tater, J. M. 1984*a* *Nature, Lond.* **307**, 23–25.
Hirn, A., Nercessian, A., Sapin, M., Jobert, G., Xu, Z.-X., Gao, E.-Y., Lu, D.-Y. & Teng, J.-W. 1984*b* *Nature, Lond.* **307**, 25–27.
Holdaway, M. J. 1971 *Am. J. Sci.* **271**, 97–131.
Hoschek, G. 1969 *Contr. Miner. Petr.* **22**, 208–232.
Jaupart, C., Francheteau, J., Shen, X.-J. 1985 *Geophys. Jl R. astr. Soc.* **81**, 131–155.
Karner, G. D. & Watts, A. B. 1983 *J. geophys. Res.* **88**, 10449–10477.
Krummenacher, D. 1971 *Géochronomètrie des roches de l'Himalaya.* In *Recherches géologiques dans l'Himalaya du Népal, région de la Thakkhola*, pp. 187–202. Paris: C.N.R.S.
Krummenacher, D., Basett, A. M., Kingery, F. A. & Layne, H. F. 1978 Petrology, metamorphism and K/Ar age determinations in Eastern Nepal. In *Tectonic geology of the Himalaya* (ed. P. S. Saklani), pp. 151–166. New Delhi: Today & Tomorrow's Printers & Publishers.
Leake, B. E. 1978 *Mineralog. Mag.* **42**, 533–563.
Le Fort, P. 1975 *Am. J. Sci.* A **275**, 1–44.
Le Fort, P. 1981 *J. geophys. Res.* **86**, 10545–10568.
Le Fort, P. 1986 *Geol. Soc. Lond.* **19**, 159–172.
Maluski, H., Proust, F. & Xiao, X.-C. 1982 *Nature, Lond.* **298**, 152–154.
Marcoux, J., De Wever, P., Nicolas, A., Girardeau, J., Xiao, X., Chang, C., Wang, N., Zao, Y., Bassoullet, J. P., Colchen, M. & Mascle, G. 1982 Preliminary report on depositional sediments on top of volcanic member: the Xigaze ophiolite (Yarlung Zangbo suture zone, China). Abstract, *Ofioliti* Suppl. **6**, 82.
Molnar, P. 1984 Structure and tectonics of the Himalaya: constraints and implications of geophysical data. *A. Rev. Earth planet. Sci.* **12**, 489–518.
Nicolas, A., Girardeau, J., Marcoux, J., Dupré, B., Xiao, X.-C., Chang, C.-F., Wang, X.-B. & Zao, Y.-G. 1981 *Nature, Lond.* **294**, 414–417.
Nur, A. & Ben-Avraham, Z. 1982 *J. geophys. Res.* **87**, 3644–3661.
Papike, J. J., Cameron, K., Baldwin, K. 1974 *Geol. Soc. Am. Program. Abstr.* **6**, 1053–1054.
Patriat, P. & Achache, J. 1984 *Nature, Lond.* **311**, 615–621.
Patriat, P., Segoufin, J., Schlich, R., Goslin, J., Auzende, J.-M., Beuzart, P., Bonnin, J. & Olivet, J. L. 1982 *Bull. Soc. géol. Fr.* **24**, 363–373.
Pécher, A. 1978 Déformations et métamorphisme associés à une zone de cisaillement. Exemple du grand chevauchement central Himalayen (M.C.T.) transversale des Annapurnas et du Manaslu, Népal. (354 pages.) These d'État, Univ. Sci. Méd. Grenoble.
Powell, C. McA. & Conaghan, P. J. 1973 *J. Geol.* **81**, 127–143.
Powell, C. McA. & Conaghan, P. J. 1975 *Geology* **3**, 727–731.
Powell, R. 1978 *Equilibrium theromodynamics in Petrology.* London: Harper & Row.
Powell, R. 1985 *J. metamorph. Geol.* **3**, 231–243.
Powell, R. & Evans, J. A. 1983 *J. metamorph. Geol.* **1**, 331–336.
Pozzi, J.-P., Westphal, M., Girardeau, J., Besse, J., Yao, X.-Z., Xian, Y.-C. & Li, S.-X. 1984 *Earth planet. Sci. Lett.* **70**, 383–394.
Qian, D., Zhang, S. & Gu, Q. 1982 *Scient. Sinica* **3**, 329–332.
Richardson, S. W., Gilbert, M. C. & Bell, P. M. 1969 *Am. Miner.* **267**, 259–272.
Schmid, S. M. 1982 Microfabric studies as indicators of deformation mechanisms and flow laws operative in mountain building. In *Mountain building processes.* (ed. K. J. Hsu), pp. 95–110. London: Academic Press.
Shackleton, R. M. 1981 *J. struct. Geol.* **3**, 97–105.
Shärer, U., Xu, R.-H., Allègre, C. J. 1984 *Earth planet. Sci. Lett.* **69**, 311–320.
Sinha-Roy, S. 1982 *Tectonophysics* **84**, 197–224.
Spear, F. S. 1981 *Am. J. Sci.* **281**, 697–734.
Storre, B. 1972 *Contr. Miner. Petr.* **37**, 87–89.
Tamaki, K. 1985 *Geology* **13**, 475–478.
Tapponnier, P., Mercier, J. L., Armijo, R., Han, T.-L. & Zhou, J. 1981 *Nature, Lond.* **294**, 410–414.
Thakur, V. C. 1980 *Tectonophysics* **62**, 141–154.

PHILOSOPHICAL TRANSACTIONS OF THE ROYAL SOCIETY A MATHEMATICAL, PHYSICAL & ENGINEERING SCIENCES

Vidal, P., Cocherie, A., Le Fort, P. 1982 *Geochim. cosmochim. Acta.* **46**, 2279–2292.
Villotte, J. P., Daignières, M. & Madariaga, R. 1982 *J. geophys. Res.* **87**, 10709–10728.
Virdi, N. S. 1981 *Tectonophysics* **72**, 141–154.
Virdi, N. S., Thakur, V. C. & Kumar, S. 1977 *Himalayan Geol.* **7**, 479–482.
Wang, J., Chen, Z., Gui, X., Xu, R. & Zhang, Y. 1981 Rb-Sr isotopic studies on some intermediate-acid plutons in southern Xizang In *Geological and ecological studies of Qinghai-Xizang plateau*, I, pp. 515–520. Beijing: Science Press.
Wells, P. R. A. 1980 *Earth planet. Sci. Lett.* **46**, 253–265.
Windley, B. R. 1983 *J. geol. Soc. Lond.* **140**, 849–865.
Winkler, H. G. F. 1974 *Petrogenesis of metamorphic rocks*. Berlin: Springer-Verlag.
Xiao, X. & Gao, Y. 1984 Some new observations on the High P/T metamorphic belt along the southern boundary of Yarlung Zangbo (Tsangpo) ophiolite zone, Xizang (Tibet) In *Himalayan geology* II: *part of achievements in geoscientific investigation of sino-french cooperation in the Himalayas in* 1981, pp. 1–18. Beijing: Geology Publishing House.
Zhang, Q., Li, D.-Z. & Li, S. H. 1981 A pair of metamorphic belts in South Xizang. In *Geological and ecological studies of the Qinghai-Xizang plateau*, I, pp. 443–450. Beijing: Science Press.
Zhang, Y-Q., Dai, T.-M. & Hong, A.-S. 1981 Isotopic geochronology of granitoid rocks in southern Xizang plateau. *Proc. Symp. Qinghai–Xizang (Tibet) plateau*, vol. **1**, pp. 483–495. Beijing: Sci. Press.

PHILOSOPHICAL TRANSACTIONS OF THE ROYAL SOCIETY A MATHEMATICAL, PHYSICAL & ENGINEERING SCIENCES